Nano Research
2022, 15(5): 3959–3963

ISSN 1998-0124 CN 11-5974/O4
https://doi.org/10.1007/s12274-022-4076-1

Research Article

Atomically dispersed Ni anchored on polymer-derived mesh-like N-doped carbon nanofibers as an efficient CO_2 electrocatalytic reduction catalyst

Tai Cao[1], Rui Lin[1], Shoujie Liu[2], Weng-Chon (Max) Cheong[3], Zhi Li[1] (✉), Konglin Wu[2], Youqi Zhu[4], Xiaolu Wang[1], Jian Zhang[1], Qiheng Li[1], Xiao Liang[1], Ninghua Fu[1], Chen Chen[1], Dingsheng Wang[1], Qing Peng[1], and Yadong Li[1] (✉)

[1] *Department of Chemistry, Tsinghua University, Beijing 100084, China*
[2] *College of Chemistry and Materials Science, Anhui Normal University, Wuhu 241000, China*
[3] *Department of Physics and Chemistry, Faculty of Science and Technology, University of Macau, Macao SAR, China*
[4] *Research Center of Materials Science, Beijing Key Laboratory of Construction Tailorable Advanced Functional Materials and Green Applications, Beijing Institute of Technology, Beijing 100081, China*

Received: 30 August 2021 / **Revised:** 11 December 2021 / **Accepted:** 15 December 2021

ABSTRACT

Efficient electroreduction of CO_2 into CO and other chemicals turns greenhouse gases into fuels and value-added chemicals, holding great promise for a closed carbon cycle and the alleviation of climate changes. However, there are still challenges in the large-scale application of CO_2 electroreduction due to the sluggish kinetics. Herein we develop a self-assembly strategy to synthesize a highly efficient CO_2 reduction electrocatalyst with atomically dispersed Ni-N_4 active centers anchored on polymer-derived mesh-like N-doped carbon nanofibers (Ni-N_4/NC). The Ni-N_4/NC exhibits high selectivity for CO_2 reduction reaction with CO Faradaic efficiency (CO FE) above 90% over a wide potential range from −0.6 to −1.0 V vs. RHE. The catalyst reaches a maximum CO FE up to 98.4% at −0.8 V with a TOF of 1.28 x 10^5 h^{-1} and Tafel slope of 113 mV·dec^{-1}. The catalyst also exhibits remarkable stability, with little change in current density and CO FE over a 10-hour durability test at –0.8 V vs. RHE. This method provides a new route for the synthesis of highly efficient CO_2 reduction electrocatalyst.

KEYWORDS

CO_2 reduction reaction, Ni-N_4 site, Ni single atoms, self-assembly

1 Introduction

The electrochemical reduction of carbon dioxide (CO_2) can store intermittent renewable energy in the form of chemical bonds and has been regarded as a promising strategy for closing the carbon cycle and storing renewable energy [1, 2]. There are great challenges to be solved for efficient carbon dioxide reduction reaction (CO_2RR). To activate CO_2, significant overpotential is required due to the high activation energy of C=O (ca. ~ 806 kJ·mol^{-1}) [3, 4]. At the same time, hydrogen evolution reaction (HER) can easily occur in aqueous electrolytes, acting as a major competitor to CO_2 reduction [5]. The development of a CO_2RR electrocatalyst with high efficiency and selectivity remains a challenge [6]. To improve the CO_2 reduction activity [7], a series of electrocatalysts including metals [8, 9] and molecular complexes [10, 11] have been explored. Molecular complexes catalysts are attractive to researchers because they have well-defined active sites [12], which facilitates the establishment of a clear structure–activity relationship for catalyst design. Among them, metalloporphyrins and phthalocyanines are widely used in CO_2RR [13], such as cobalt phthalocyanine (CoPc) and cobalt tetraphenylporphyrin (CoTPP), owing to their high activity and selectivity [14].

Recently, porphyrin metal complexes anchored on N-doped carbon materials have been investigated as CO_2RR electrocatalysts [15]. Adsorption of porphyrin metal complex from solution onto the support surface is the most common method for supporting catalysts [16]. However, due to the π-conjugation, which leads to the adsorption of several layers of π–π stacking, a proportion of metalloporphyrins molecules may become unreactive and even agglomerate into metal particles during synthetic procedures.

Herein, we develop a self-assembly strategy to synthesize a highly efficient CO_2RR electrocatalyst with atomically dispersed Ni sites anchored on mesh-like N-doped carbon nanofibers derived from polymer with a high surface area (332 $m^2 \cdot g^{-1}$). The catalyst is synthesized by anchoring nickel phthalocyanine-tetrasulfonic acid tetrasodium salt (NiPcTs), a Ni precursor with a well-defined Ni-N_4 structure, on polypyrrole via hydrogen bonding and electrostatic interactions. This synthetic route drives the self-assembly of NiPcTs and polypyrrole into a one-dimensional carbon fiber network material and avoids the loss of active sites caused by the π–π stacking of metal-phthalocyanine. Electrochemical measurements show that the catalyst exhibits excellent electrocatalytic activity and stability for CO_2 reduction. The catalyst reaches a maximum CO FE up to 98.4% at –0.8 V with a TOF of 1.28 × 10^5 h^{-1} and 113 mV·dec^{-1} Tafel slope. Moreover, the CO FE of the catalyst can be maintained above 90% within a wide potential window of –0.6 to –1.0 V.

Address correspondence to Zhi Li, leejn18@foxmail.com; Yadong Li, ydli@tsinghua.edu.cn

2 Experimental details

2.1 Chemicals

Nickel phthalocyanine-tetrasulfonic acid tetrasodium salt, nickel phthalocyanine (NiPc), and tetraethoxysilane (TEOS) were purchased from Aldrich. N,N-Dimethylformamide (DMF, AR) was purchased from Beijing Chemical Works. F127 (PEO106PPO70PEO106) was purchased from Sigma. Resorcinol (99%) and melamine (99%) were purchased from J&K Scientific Ltd. Formaldehyde, pyrrole, and ammonium persulphate were purchased from Alfa. Sodium bicarbonate (99.999%) was purchased from Acros. FuelCellsEtc provided the carbon paper (325 μm thickness) sigracet 39BC; Nafion 117 membrane was purchased from Dupont. From the milli-Q system, 18.2 MΩ·cm ultrapure water was derived.

2.2 Synthesis of Ni-N_4/NC

Ni-N_4/NC was prepared through a self-assembly strategy. Firstly, 103 μL pyrrole was dissolved in 1.5 mL isopropanol (solution A), and then 0.342 g ammonium persulphate and 35 mg nickel phthalocyanine-tetrasulfonic acid tetrasodium salt was dissolved in 3 mL deionized water to prepare solution B. The solution A and B were cooled to 4 °C in an ice bath and then rapidly mixed. To remove excess ions, purification of the product was accomplished through a 24-hour consecutive immersion in ethanol and deionized water. The product was collected by centrifugation and then treated with liquid nitrogen and freeze-dried to obtain the aerogel. Finally, the resulting black aerogel was heated to 800 °C under a nitrogen atmosphere for 120 min and cooled to room temperature naturally to obtain Ni-N_4/NC. The Ni content (determined by ICP-OES) is 0.1 wt.%.

2.3 Synthesis of electrocatalyst with Ni-N_5 active sites

As a comparison with the Ni-N_4/NC, Ni-N_5 on polymer-derived hollow N-doped porous carbon spheres (HNPCSs) was synthesized according to a reported method [17]. 2.5 mL ammonia aqueous solution, 60 mL ethanol, and 20 mL deionized water were mixed and agitated at 30 °C for 30 min. Subsequently, 2.8 mL of TEOS was slowly injected into the above mixture for 30 min. After that, 0.3 g of F127, 0.4 g of resorcinol, and 0.56 mL of formaldehyde were added to the above mixture and stirred for 30 min. Later, 0.315 g of melamine and 0.42 mL of formaldehyde were added. The color of the solution gradually changed from white to brown. The above mixture was stirred for 24 h. After transferring the aforesaid mixture to a 100 mL Teflon-lined stainless steel autoclave, it was heated to 100 °C for 24 h. The resulting product was centrifuged and rinsed three times with ethanol and deionized water. Finally, the products were dried in an oven at 80 °C for 12 h to obtain SiO_2@melamine-resorcinol-formaldehyde polymer spheres (SiO_2@MRFPSs). The obtained SiO_2@MRFPSs powder was heated to 700 °C with a heating rate of 2 °C·min^{-1} and kept at 700 °C for 2 h under flowing Ar gas. After cooled to room temperature, HNPCSs were obtained by etching the SiO_2 of the carbonized products with hydrofluoric acid (15 wt.%) for 48 h. 30 mg of HNPCSs and 20 mg of NiPc were dispersed in 30 mL of DMF and sonicated for at least 1 h, respectively. Then, NiPc-DMF dispersion solution was added to the HNPCSs-DMF suspension. The suspension was agitated for 24 h at room temperature. Then, the Ni-N_5/HNPCSs catalyst was obtained after vacuum filtration, washing with DMF and ethanol several times, and drying in a vacuum oven at 60 °C for 12 h. The Ni content (determined by inductively coupled plasma optical emission spectrometry (ICP-OES)) is 2.9 wt.%.

2.4 Material characterization

Characterization: The morphology of as-prepared samples were characterized by transmission electron microscopy (TEM, Hitachi HT7700), high-resolution transmission electron microscopy (HRTEM, FEI Tecnai G2 F20 S-Twin) and the aberration-corrected high-resolution transmission electron microscopy (AC-STEM, Titan Cubed Themis 60-300). X-ray diffraction (XRD) data were collected by a monochromatized Cu K radiation on the Bruker D8 X-ray diffractometer (Cu Kα radiation: λ = 0.15406 nm). X-ray photoelectron spectroscopy (XPS) measurements were performed on the PHI Quantro SXM spectrometer. The binding energy (BE) of sample was calibrated by setting the observed binding energy of C 1s to 284.8 eV. ICP-OES data were obtained on Thermo Fisher IRIS Intrepid II. The analysis of CO was performed by temperature-programmed desorption mass spectrometry (TPD-MS) on the Auto Chem TM II 2920-OmniStar GSD320 equipment. Raman spectra were taken using a Horiba JY HR-800 confocal Raman microscope with a 514 nm excitation laser under an intensity of 5 mW. Scanning electron microscope (SEM) images were recorded using a Sirion 200 field emission scanning electron microscope. The X-ray absorption fine structure (XAFS) spectra data were collected on a 1W1B station in Beijing Synchrotron Radiation Facility (BSRF, operated at 2.5 GeV with a maximum current of 250 mA Ni K-edge). The XAFS data of Ni electrocatalyts samples were collected at room temperature in fluorescence excitation mode and all the references (metal and oxide bulks) were recorded in transmission mode using ionization chamber. All samples were pelletized as disks of 13 mm diameter with 1mm thickness using graphite powder as a binder. The acquired EXAFS data were processed according to the standard procedures using the ATHENA module implemented in the IFEFFIT software packages.

2.5 Electrochemical CO_2 reduction experiment

A 0.1 M $NaHCO_3$ aqueous solution (pH = 6.8) was obtained by pouring carbon dioxide gas into the sodium carbonate aqueous solution overnight. The electrolyzer for CO_2 electrochemical reduction was an H-type cell. A Nafion 117 membrane was set between the cathodic and anodic chambers. The CO_2 flow rate was regulated to 20 sccm using a mass flow controller. The sigracet 39BC carbon paper, Pt wire, and Ag/AgCl were utilized as the working, counter, and reference electrodes, respectively. Linear sweep voltammetry (LSV) curves were recorded by using the Princeton PMC-500 electrochemical workstation at a scan rate of ten millivolts per second. Electrochemical impedance spectroscopy (EIS) studies were performed at a potential of 5 mV against open circuit potential. The potential value has been converted to a number versus the reversible hydrogen electrode (RHE). Chronoamperometry measurements were performed for 40 min at each potential. The electrolysis gas products were detected by using a Shimazu 2010 plus gas chromatography system equipped with a BID detector and a ShinCarbon ST 100/120 packed column. The helium of extremely high purity (99.9999%) was employed as the carrier gas in the chromatography. The liquid products of electrolysis were analyzed by Bruker Avance Ⅲ HD 400 NMR. The equation calculated the Faraday efficiency of gas products:

$$FE = \frac{2 \times 96,485\ (C \cdot mol^{-1}) \times V\ (mL \cdot min^{-1}) \times 10^{-6}\ (m^3 \cdot mL^{-1}) \times v(vol.\%) \times 10^5 (Pa)}{8.314\ (J \cdot mol^{-1} \cdot K^{-1}) \times 298.15(K) \times I_{total}\ (C \cdot s^{-1}) \times 60\ (s \cdot min^{-1})}$$

v (vol.%) = CO volume concentration in the cell's exhaust gas. V (mL·min^{-1}) = at room temperature and pressure, the gas flow

rate was determined using a flow meter at the cell's outlet.

I_{total} ((C·s^{-1}) = cell current in a constant condition.

The TOF value of the electrocatalyst was calculated according to the formula:

$$\mathrm{TOF} = \frac{I_{\mathrm{product}}/nF}{m_{\mathrm{cat}}\omega/M_{\mathrm{Ni}}} \times 3,600$$

TOF: turnover frequency, h^{-1}.

$I_{product}$: partial current for a certain product, A.

n: the number of electrons transferred for product formation, which is 2 for both CO and H_2 production.

F: Faradaic constant, 96,485 C·mol^{-1}.

m_{cat}: catalyst mass in the electrode, g.

ω: Ni loading in the catalyst.

M_{Ni}: atomic mass of Ni, 58.69 g·mol^{-1}.

3 Results and discussion

As shown in the schematic illustration (Scheme l), NiPcTs act as dopants and cross-linkers to assemble polypyrrole (PPy) polymer chains into one-dimensional structured nanotubes through electrostatic interactions and hydrogen bonding between the NiPcTs and PPy chains. These one-dimensional nanotubes are interwoven to form a mesh-like structure. The reticulated sample was pyrolyzed at 800 degrees under argon to give Ni-N_4/NC catalysts. NiPcTs are not stacked owing to their hydrogen bonding and electrostatic interactions with polypyrrole chains, preventing agglomeration during the pyrolysis at high temperature.

The morphology of Ni-N_4/NC and Ni-N_5/HNPCSs is studied by SEM and TEM. Ni-N_4/NC catalyst consists of uniformly interconnected nanofibers of approximately 50 nm in diameter, featuring a three-dimensional mesh structure as can be seen in Figs. 1(a) and 1(b). The morphology of Ni-N_5/HNPCSs are characterized with hollow porous spheres (Fig. S1 in the Electronic Supplementary Material (ESM)). HAADF-STEM and EDS images show that Ni are uniformly distributed over the entire Ni-N_4/NC (Fig. 1(c)) and Ni-N_5/HNPCSs nanostrucure (Fig. S2 in the ESM). No sign of aggregated Ni species can be observed. AC-STEM images confirm the Ni species of both Ni-N_4/NC and Ni-N_5/HNPCSs are atomically dispersed on the support (high density of bright spots marked with red circles in Fig. 1(d) and Fig. S3 in the ESM).

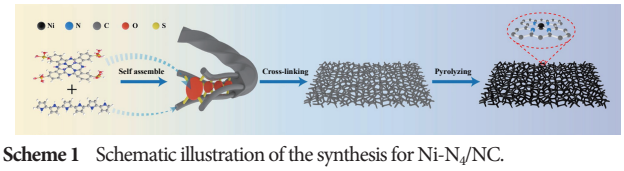

Scheme 1 Schematic illustration of the synthesis for Ni-N_4/NC.

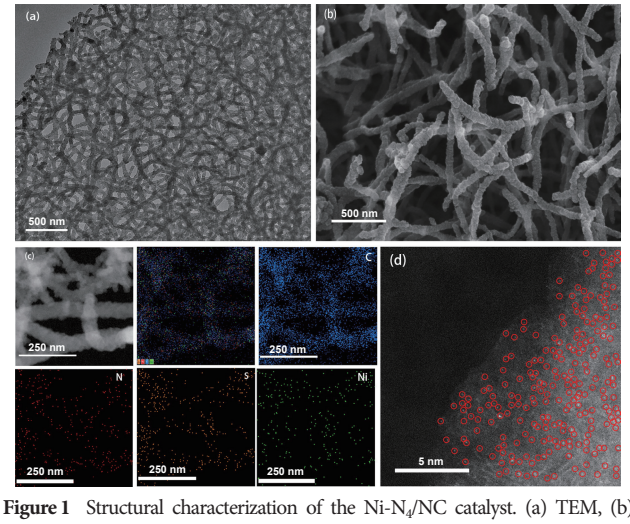

Figure 1 Structural characterization of the Ni-N_4/NC catalyst. (a) TEM, (b) SEM, (c) HAADF-STEM and EDS mapping images, C (blue), N (red), S (yellow), and Ni (green), (d) AC-STEM image of the Ni-N_4/NC catalyst. Single Ni atoms are highlighted with red circles in the AC HAADF-STEM image.

The XRD patterns of Ni-N_4/NC and Ni-N_5/HNPCSs both show broad peaks located at about 25°, corresponding to the characteristic carbon (002) diffraction (Fig. 2(a)) [18]. The Ni-N_4/NC with three-dimensional mesh structure possesses an effective BET surface area of 332 m^2·g^{-1}, smaller than that of Ni-N_5/HNPCSs with hollow porous spheres structure (513 m^2·g^{-1}) (Fig. 2(b)). XPS measurements were conducted to verify the surface components and valence states of Ni-N_4/NC and Ni-N_5/HNPCSs. As shown in Fig. 2(c), the Ni 2p spectrum of Ni-N_4/NC indicates that the Ni oxidation state lies between Ni^0 (853.0 eV) and Ni^{2+} (855.7 eV) whereas Ni-N_5/HNPCSs shows Ni oxidation state close to Ni^{2+} (855.7 eV) (Fig. S4 in the ESM) [19, 20]. The N 1s spectrum of Ni-N_4/NC (Fig. 2(d)) can be fitted to four typical peaks corresponding to pyridine N (398.3 eV), metal-N (399.1 eV), and pyrrole N (400.9 eV).

To better understand the electronic structure and coordination environment, X-ray absorption spectroscopy (XAS) experiments were performed on the Ni CO_2RR electrocatalysts. According to the Ni K-edge XANES pattern in Fig. 3(a), the Ni species in Ni-N_4/NC have a higher oxidation state than Ni foil and lower oxidation state than NiO [21, 22], which is in accordance with the XPS results. Fourier transformation of the EXAFS (FT-EXAFS) spectrum (Fig. 3(b)) of Ni-N_4/NC shows a dominant peak at 1.4 Å due to scattering interaction between Ni atoms and the first shell (Ni-N) [23]. The absence of a Ni-Ni peak at 2.15 Å indicates the atomic dispersion of Ni atoms on Ni-N_4/NC, which is consistent with the AC-STEM results [24]. In order to gain further insight into the coordination environment and chemical structure of Ni species in the catalysts, FT EXAFS spectra were fitted in R (Fig. 3(c)) and k space (Fig. S5 in the ESM). Central Ni has a coordination number of 3.7 and bond lengths of about 2.0 (Table S1 in the ESM), indicating the presence of Ni-N_4 coordination structures [25]. The K-edge FT-EXAFS of Ni-N_5/HNPCSs also demonstrates the atomically dispersion of Ni on the support (Fig. S6 in the ESM) and the fitting results of the EXAFS spectra of Ni-N_5/HNPCSs indicates a central Ni with coordination number of 5.2 (Table S1 in the ESM).

CO_2RR measurements are performed in an aqueous $NaHCO_3$ solution saturated with CO_2 (0.1 M). The LSV technique is used to measure all samples. CO and H_2 are the main products of the

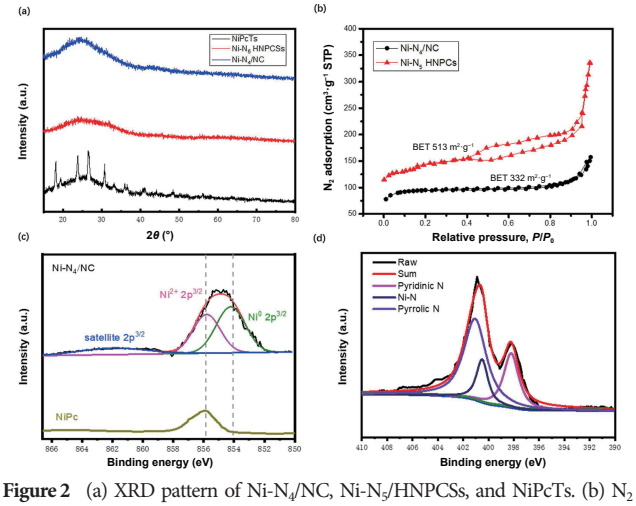

Figure 2 (a) XRD pattern of Ni-N_4/NC, Ni-N_5/HNPCSs, and NiPcTs. (b) N_2 adsorption-desorption isotherm of Ni-N_4/NC and Ni-N_5/HNPCSs. (c) XPS spectra of Ni-N_4/NC and NiPc for Ni 2p regions. (d) XPS spectra of Ni-N_4/NC for N 1s regions.

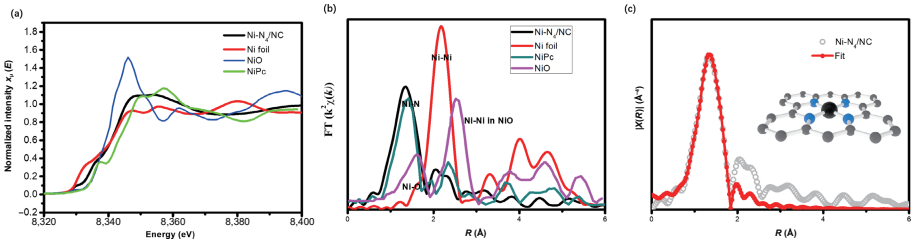

Figure 3 (a) XANES spectra at the Ni K-edge of Ni-N_4/NC, NiO, NiPc, and Ni foil, respectively. (b) FT-EXAFS spectra of Ni-N_4/NC, NiO, NiPc, and Ni foil, respectively. (c) The fitting results of the EXAFS spectra of Ni-N_4/CN in *k* space.

CO_2RR process and no additional compounds are detected by using ^{1}H nuclear magnetic resonance in the electrolyte for Ni-N_4/NC [26] (Fig. S7 in the ESM). The LSV curves demonstrate that the current response of Ni-N_4/NC to CO_2 reduction is significantly greater than that of Ni-N_5 HNPCSs and NiPc (Fig. 4(a)). For Ni-N_4/NC, a CO signal is detected starting at –0.40 V vs. RHE, which indicates that the CO_2 onset overpotential for CO is at least below 280 mV. Meanwhile, the CO FE of the catalyst can be maintained above 90% within a wide potential window of –0.6 to –1.0 V vs. RHE. Ni-N_4/NC exhibits a maximum CO FE up to 98.4% at –0.8 V. In addition, the CO partial current density (J_{CO}) of Ni-N_4/NC at –0.8 V vs. RHE is 14.43 mA/cm^2 (Fig. S8 in the ESM), with a TOF of 1.28×10^5 h^{-1}, much higher than that of Ni-N_5/HNPCSs (2.08×10^3 h^{-1}) and NiPc (Fig. S9 in the ESM). The morphology of Ni-N_4 and Ni-N_5 catalysts are characterized with mesh-like nanofibers and hollow porous spheres, respectively (Fig. 1(b), Figs. S1 and S2 in the ESM). Although their morphology and specific surface area are different, the normalization of their performance to the activity of a single Ni (TOF) can reflect their intrinsic activity difference. The Tafel slope of Ni-N_4/NC was 113 mV·dec^{-1} (Fig. 4(c)), which is smaller than the slopes of Ni-N_5/HNPCSs and NiPc, indicating that Ni-N_4/NC is more favorable for the kinetics of CO_2 reduction reaction [27]. We suppose that the better performance of Ni-N_4 stems from its electronic and geometric structure which is more conducive to CO_2 adsorption and reduction. The coordination of Ni-N_4 is more unsaturated than that of Ni-N_5, providing suitable sites for CO_2 adsorption and reduction. Moreover, Ni-N_4/NC also shows less resistance to charge transfer than Ni-N_5/HNPCSs, which further supports its higher catalytic activity (Fig. S10 in the ESM) [28]. The influence of calcination temperature on the CO_2 activity of catalysts is also investigated [29]. A pyrolysis temperature of 800 °C is ideal for CO_2 performance. Although Ni-N_4/NC-700 exhibits similar FE CO with Ni-N_4/NC-800, the latter shows an advantage in current density (Figs. S11 and S12 in the ESM). In addition, Ni-N_4/NC exhibits ultra-high stability with little change in current density and CO FE over a 10-hour period at –0.8 V (Fig. 4(d)). These results demonstrate the catalytic performance of Ni-N_4/NC with Ni-N_4 coordination structures is much higher than that of Ni-N_5 coordination structure catalyst for CO_2RR, emphasizing the critical importance of the coordination environment for single atom sites electrocatalysis [30].

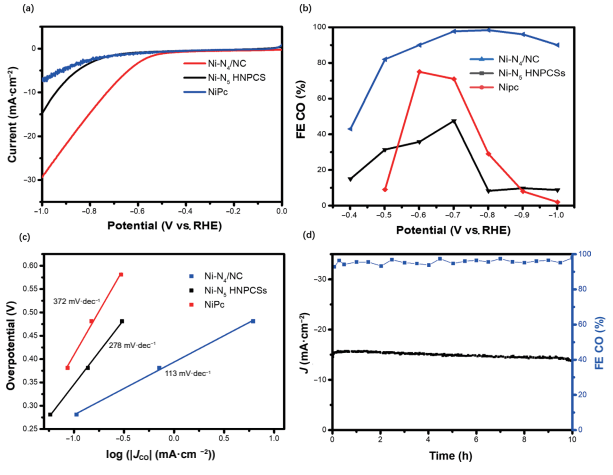

Figure 4 (a) LSV curves, (b) faradaic efficiencies, and (c) Tafel plots of Ni-N_4/NC, Ni-N_5 HNPCSs and NiPc in CO_2-saturated 0.1 M $NaHCO_3$. (d) The stability tests of Ni-N_4/NC at –0.8 V vs. RHE.

4 Conclusions

In conclusion, we have developed a simple and effective approach for the synthesis of atomically dispersed Ni atoms anchored on mesh-like N-doped carbon nanofibers generated from polymers. The Ni-N_4/NC are synthesized by anchoring well-defined NiPcTs structures to polypyrrole molecular chains via hydrogen bonding and electrostatic interactions followed by high-temperature treatment. The Ni-N_4/NC exhibits excellent electrocatalytic activity and ultra-high stability for CO_2 reduction. The catalyst reaches a maximum CO FE up to 98.4% at –0.8 V with a TOF of 1.28×10^5 h^{-1} and 113 mV·dec^{-1} Tafel slope, much superior to that of Ni-N_5/HNPCSs. Additionally, the CO FE of Ni-N_4/NC can be maintained above 90% over a broad potential range of –0.6 to –1.0 V. We believe this work will deepen the understanding of the coordination microenvironment modification of single-atom Ni sites for electrocatalysis, as well as the manufacture of single-atom catalysts anchored on a polymer-based substrate for efficient CO_2RR.

Acknowledgements

This work was supported by the National Key R&D Program of China (No. 2018YFA0702003), the National Natural Science Foundation of China (Nos. 21890383 and 21971137) and Beijing Municipal Science & Technology Commission (No. Z191100007219003).

Electronic Supplementary Material: Supplementary material (SEM, HADDF-STEM and mapping imaging and Raman spectroscopy measurements, etc.) is available in the online version of this article at https://doi.org/10.1007/s12274-022-4076-1.

References

[1] Gu, J.; Hsu, C. S.; Bai, L. C.; Chen, H. M.; Hu, X. L. Atomically dispersed Fe^{3+} sites catalyze efficient CO_2 electroreduction to CO. *Science* **2019**, *364*, 1091–1094.

[2] Nitopi, S.; Bertheussen, E.; Scott, S. B.; Liu, X. Y.; Engstfeld, A. K.; Horch, S.; Seger, B.; Stephens, I. E. L.; Chan, K.; Hahn, C. et al. Progress and perspectives of electrochemical CO_2 reduction on copper in aqueous electrolyte. *Chem. Rev.* **2019**, *119*, 7610–7672.

[3] Zheng, T. T.; Jiang, K.; Wang, H. T. Recent advances in electrochemical CO_2-to-CO conversion on heterogeneous catalysts. *Adv. Mater.* **2018**, *30*, 1802066.

[4] Birdja, Y. Y.; Pérez-Gallent, E.; Figueiredo, M. C.; Göttle, A. J.;

Calle-Vallejo, F.; Koper, M. T. M. Advances and challenges in understanding the electrocatalytic conversion of carbon dioxide to fuels. *Nat. Energy* **2019**, *4*, 732–745.

[5] Su, X.; Yang, X. F.; Huang, Y. Q.; Liu, B.; Zhang, T. Single-atom catalysis toward efficient CO_2 conversion to CO and formate products. *Acc. Chem. Res.* **2019**, *52*, 656–664.

[6] Chen, W. Y.; Liu, X. M.; Han, B.; Liang, S. J.; Deng, H.; Lin, Z. Boosted photoreduction of diluted CO_2 through oxygen vacancy engineering in NiO nanoplatelets. *Nano Res.* **2020**, *14*, 730–737.

[7] Liang, S. J.; Liu, X. M.; Zhong, Z. Q.; Han, B.; Zhong, X. H.; Chen, W. Y.; Song, K. N.; Deng, H.; Lin, Z. Lattice-strained nanotubes facilitate efficient natural sunlight-driven CO_2 photoreduction. *Nano Res.* **2020**, *14*, 2558–2567.

[8] Lin, R.; Ma, X. L.; Cheong, W. C.; Zhang, C.; Zhu, W.; Pei, J. J.; Zhang, K. Y.; Wang, B.; Liang, S. Y.; Liu, Y. X. et al. PdAg bimetallic electrocatalyst for highly selective reduction of CO_2 with low COOH* formation energy and facile CO desorption. *Nano Res.* **2019**, *12*, 2866–2871.

[9] Zhang, N. Q.; Zhang, X. X.; Tao, L.; Jiang, P.; Ye, C. L.; Lin, R.; Huang, Z. W.; Li, A.; Pang, D. W.; Yan, H. et al. Silver single-atom catalyst for efficient electrochemical 2 reduction synthesized from thermal transformation and surface reconstruction. *Angew. Chem., Int. Ed.* **2021**, *60*, 6170–6176.

[10] Corbin, N.; Zeng, J.; Williams, K.; Manthiram, K. Heterogeneous molecular catalysts for electrocatalytic CO_2 reduction. *Nano Res.* **2019**, *12*, 2093–2125.

[11] Jiang, Z. L.; Wang, T.; Pei, J. J.; Shang, H. S.; Zhou, D. N.; Li, H. J.; Dong, J. C.; Wang, Y.; Cao, R.; Zhuang, Z. B. et al. Discovery of main group single Sb-N_4 active sites for CO_2 electroreduction to formate with high efficiency. *Energy Environ. Sci.* **2020**, *13*, 2856–2863.

[12] Cheng, Y.; Veder, J. P.; Thomsen, L.; Zhao, S. Y.; Saunders, M.; Demichelis, R.; Liu, C.; De Marco, R.; Jiang, S. P. Electrochemically substituted metal phthalocyanines, e-MPc (M = Co, Ni), as highly active and selective catalysts for CO_2 reduction. *J. Mater. Chem. A* **2018**, *6*, 1370–1375.

[13] Chen, J. Y.; Wang, T. T.; Li, Z. J.; Yang, B.; Zhang, Q. H.; Lei, L. C.; Feng, P. Y.; Hou, Y. Recent progress and perspective of electrochemical CO_2 reduction towards C_2-C_5 products over non-precious metal heterogeneous electrocatalysts. *Nano Res.* **2021**, *14*, 3188–3207.

[14] Sorokin, A. B. Phthalocyanine metal complexes in catalysis. *Chem. Rev.* **2013**, *113*, 8152–8191.

[15] Zhang, X.; Wang, Y.; Gu, M.; Wang, M. Y.; Zhang, Z. S.; Pan, W. Y.; Jiang, Z.; Zheng, H. Z.; Lucero, M.; Wang, H. L. et al. Molecular engineering of dispersed nickel phthalocyanines on carbon nanotubes for selective CO_2 reduction. *Nat. Energy* **2020**, *5*, 684–692.

[16] Ma, Z. J.; Zhang, X. L.; Han, X. Y.; Wu, D. P.; Wang, H. J.; Gao, Z. Y.; Xu, F.; Jiang, K. Synergistic adsorption and activation of nickel phthalocyanine anchored onto ketjenblack for CO_2 electrochemical reduction. *Appl. Surf. Sci.* **2021**, *538*, 148134.

[17] Pan, Y.; Lin, R.; Chen, Y. J.; Liu, S. J.; Zhu, W.; Cao, X.; Chen, W. X.; Wu, K. L.; Cheong, W. C.; Wang, Y. et al. Design of single-atom Co-N_5 catalytic site: A robust electrocatalyst for CO_2 reduction with nearly 100% CO selectivity and remarkable stability. *J. Am. Chem. Soc.* **2018**, *140*, 4218–4221.

[18] Pan, Y.; Liu, S. J.; Sun, K. A.; Chen, X.; Wang, B.; Wu, K. L.; Cao, X.; Cheong, W. C.; Shen, R. A.; Han, A. J. et al. A bimetallic Zn/Fe polyphthalocyanine-derived single-atom Fe-N_4 catalytic site: A superior trifunctional catalyst for overall water splitting and Zn-air batteries. *Angew. Chem., Int. Ed.* **2018**, *57*, 8614–8618.

[19] Yang, X.; Cheng, J.; Fang, B. Z.; Xuan, X. X.; Liu, N.; Yang, X.; Zhou, J. H. Single Ni atoms with higher positive charges induced by hydroxyls for electrocatalytic CO_2 reduction. *Nanoscale* **2020**, *12*, 18437–18445.

[20] Zhang, Y.; Jiao, L.; Yang, W. J.; Xie, C. F.; Jiang, H. L. Rational fabrication of low-coordinate single-atom Ni electrocatalysts by mofs for highly selective CO_2 reduction. *Angew. Chem., Int. Ed.* **2021**, *133*, 7686–7689.

[21] Fan, Q.; Hou, P. F.; Choi, C.; Wu, T. S.; Hong, S.; Li, F.; Soo, Y. L.; Kang, P.; Jung, Y.; Sun, Z. Y. Activation of Ni particles into single Ni-N atoms for efficient electrochemical reduction of CO_2. *Adv. Energy Mater.* **2020**, *10*, 1903068.

[22] Zheng, T. T.; Jiang, K.; Ta, N.; Hu, Y. F.; Zeng, J.; Liu, J. Y.; Wang, H. T. Large-scale and highly selective CO_2 electrocatalytic reduction on nickel single-atom catalyst. *Joule* **2019**, *3*, 265–278.

[23] Prslja, P.; López, N. Stability and redispersion of Ni nanoparticles supported on N-doped carbons for the CO_2 electrochemical reduction. *ACS Catal.* **2021**, *11*, 88–94.

[24] Cheng, Y.; Zhao, S. Y.; Johannessen, B.; Veder, J. P.; Saunders, M.; Rowles, M. R.; Cheng, M.; Liu, C.; Chisholm, M. F.; De Marco, R. et al. Atomically dispersed transition metals on carbon nanotubes with ultrahigh loading for selective electrochemical carbon dioxide reduction. *Adv. Mater.* **2018**, *30*, 1706287.

[25] Li, X. G.; Bi, W. T.; Chen, M. L.; Sun, Y. X.; Ju, H. X.; Yan, W. S.; Zhu, J. F.; Wu, X. J.; Chu, W. S.; Wu, C. Z. et al. Exclusive Ni-N_4 sites realize near-unity CO selectivity for electrochemical CO_2 reduction. *J. Am. Chem. Soc.* **2017**, *139*, 14889–14892.

[26] Tan, D. X.; Zhang, J. L.; Yao, L.; Tan, X. N.; Cheng, X.; Wan, Q.; Han, B. X.; Zheng, L. R.; Zhang, J. Multi-shelled CuO microboxes for carbon dioxide reduction to ethylene. *Nano Res.* **2020**, *13*, 768–774.

[27] Jiang, K.; Siahrostami, S.; Zheng, T. T.; Hu, Y. F.; Hwang, S.; Stavitski, E.; Peng, Y. D.; Dynes, J.; Gangisetty, M.; Su, D. et al. Isolated Ni single atoms in graphene nanosheets for high-performance CO_2 reduction. *Energy Environ. Sci.* **2018**, *11*, 893–903.

[28] Xiong, W. F.; Li, H. F.; Wang, H. M.; Yi, J. D.; You, H. H.; Zhang, S. Y.; Hou, Y.; Cao, M. N.; Zhang, T.; Cao, R. Hollow mesoporous carbon sphere loaded Ni-N_4 single-atom: Support structure study for CO_2 electrocatalytic reduction catalyst. *Small* **2020**, *16*, 2003943.

[29] Cao, T.; Wang, D. S.; Zhang, J. T.; Cao, C. B.; Li, Y. D. Bamboo-like nitrogen-doped carbon nanotubes with Co nanoparticles encapsulated at the tips: Uniform and large-scale synthesis and high-performance electrocatalysts for oxygen reduction. *Chemistry* **2015**, *21*, 14022–14029.

[30] Rong, X.; Wang, H. J.; Lu, X. L.; Si, R.; Lu, T. B. Controlled synthesis of a vacancy-defect single-atom catalyst for boosting CO_2 electroreduction. *Angew. Chem., Int. Ed.* **2020**, *59*, 1961–1965.